Case Studies in Thermal Engineering 59 (2024) 104452

Contents lists available at ScienceDirect

Case Studies in Thermal Engineering

journal homepage: www.elsevier.com/locate/csite

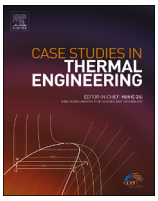

Maximizing thermal and electrical efficiency with thermoelectric generators and hybrid photovoltaic converters: Numerical, economic, and machine learning analysis

Haitham Osman [a], Loke Kok Foong [b, c, **], Binh Nguyen Le [b, c], Velibor Spalevic [d, e], Branislav Dudic [f, g, *], Goran Skataric [h, i]

[a] Department of Chemical Engineering, College of Engineering, King Khalid University, Abha, 61411, Saudi Arabia
[b] Institute of Research and Development, Duy Tan University, Da Nang, Viet Nam
[c] School of Engineering & Technology, Duy Tan University, Da Nang, Viet Nam
[d] Biotechnical Faculty, University of Montenegro, 81000, Podgorica, Montenegro
[e] Faculty of Philosophy, Geography, University of Montenegro, 81400, Niksic, Montenegro
[f] Faculty of Management, Comenius University Bratislava, 81499, Bratislava, Slovakia
[g] Faculty of Economics and Engineering Management, University Business Academy, 21000, Novi Sad, Serbia
[h] Management, Maritime Faculty, University of Montenegro, 85331, Kotor, Montenegro
[i] Marketing, Faculty of Sports and Physical Education, University of Montenegro, 81400, Niksic, Montenegro

ARTICLE INFO

Handling Editor: Huihe Qiu

Keywords:
Hybrid system
Photovoltaic-thermoelectric
Solar absorption
Power generation
Artificial neural network

ABSTRACT

In this paper, we introduce an innovative thermoelectric, photovoltaic hybrid system and investigate its performance under various radiation intensities and heat transfer coefficients outside the cavity. Our findings reveal that the proposed system yields twice the power output compared to a traditional plate thermoelectric, photovoltaic hybrid system. Through economic analysis, we project a 45 % reduction in energy cost with this novel structure compared to a full hybrid system. Notably, positioning the hybrid system at the bottom of the cavity, where maximum radiation occurs, is deemed optimal. Our heat transfer analysis demonstrates a significant increase in power generation due to convection outside the cavity, with approximately 9 % of incoming radiation reflected and a further 59 % reflected without the cavity. Utilizing artificial neural networks, we predict thermal and electrical power generation, achieving a Mean Absolute Error (MAE) below 3 % and an R-squared value exceeding 0.98. Additionally, our model's predictions closely match experimental results, validating its accuracy and practical utility. This comprehensive study advances the field by offering a novel hybrid system design that outperforms existing solutions while providing insights into optimizing placement and enhancing power generation through sophisticated modeling techniques.

1. Introduction

The net production of electrical energy in 2012 was 21.6 billion megawatt hours, which according to the forecast of the International Energy Outlook (2016) report, this amount will increase to 36.5 billion megawatt hours in the year 2040, which shows its

* Corresponding author. Faculty of Economics and Engineering Management, University Business Academy, 21000, Novi Sad, Serbia.
** Corresponding author. Institute of Research and Development, Duy Tan University, Da Nang, Viet Nam.
E-mail addresses: Haman@kku.edu.sa (H. Osman), lokekokfoong@duytan.edu.vn (L. Kok Foong), bnlnguyen@duytan.edu.vn (B. Nguyen Le), velibor.spalevic@gmail.com (V. Spalevic), branislav.dudic@fm.uniba.sk (B. Dudic), goran.skataric@yahoo.com (G. Skataric).

https://doi.org/10.1016/j.csite.2024.104452
Received 17 June 2023; Received in revised form 19 April 2024; Accepted 26 April 2024
Available online 27 April 2024

growth [1,2]. In other words, today, energy consumption has reached more than 43 TW h, of which more than 87 % is provided by fossil fuels [3,4]. Several efforts have been made to utilize renewable energy to meet the rapidly growing electricity demand and avoid harmful environmental effects caused by fossil fuels [5,6].

The production of pure electrical energy from renewable sources will grow by an average of 2.9 % annually between 2012 and 2040 [7]. There are two methods for supplying electricity from solar energy [8]. Thermal and photovoltaic systems are two methods of converting the sun's energy into electricity. Photovoltaic cells are high-efficiency converters that are affected by heat, and their efficiency decreases as the working temperature increases. One of the ways to reduce the power loss caused by the increase in cell temperature is by using a combined thermal photovoltaic system. In this system, the heat of the photovoltaic cell is passed to a heat exchanger sink. A thermoelectric generator is one of the new converters that can be used in this hybrid system. These generators have a lower power-to-mass ratio than other energy production methods, and because they do not have moving parts, they have high reliability and require less maintenance [9]. In the following, the studies on these hybrid systems are presented.

Using photovoltaic modules, thermoelectric modules, and heat extraction channels with or without concentrators, Gao et al. [10] investigated four types of systems. Temperature differences ranging from 50 to 200 °C were investigated for the studied bismuth trillium thermoelectric generators. They found that at a temperature difference of 155 °C, the efficiency of the thermoelectric generator reaches about 4 %. Li et al. [11] investigated the effect of a splitter in a photovoltaic/thermoelectric generator hybrid system. They concluded that the total power increased by 43 %. Alimoradi et al. [12] produce electricity and heat simultaneously using a thermoelectric generator coupled with linear parabolic solar collectors. As a result of this generator's temperature gradient transfers heat from the upper to the lower cycle for storage by a thermosiphon system used in this research as a heat absorber. As part of their study, various types of thermoelectric generators, such as bismuth telluride, lead telluride, and silicon germanium, have been examined, as well as the effects of various materials on the working fluid of the system and the body of the thermosiphon. In other studies [13,14] utilized secondary reflector temperature for thermoelectric generator modules. They observed that by increasing the radiation intensity, the temperature of the reflector and the efficiency of the thermoelectric modules increased. Jalili et al. [15] explored transient squeezing flow in 2D Magnetohydrodynamics (MHD) with Casson fluid under solar irradiance, investigating heat and mass transition. In another research [16], they investigated convective flow of a constant, laminar, incompressible viscous fluid over a moving plate with added nanoparticles like Al and Cu. Heat transfer effects such as radiation, internal heat generation, and viscous dissipation were also considered.

In Li et al.'s study [17], a thermoelectric generator is attached to a solar cell. Using existing methods to separate solar wavelengths, this system can use a wide range of solar radiation. Solar cells receive short wavelengths from the sun, while thermoelectric generators receive long ones. Overall efficiency is high due to the combination of both. They also investigated various thermoelectric parameters. Efficiencies increase with increasing temperature gradients. Optimizing and arranging system components is essential to increase efficiency [18,19].

Using thermoelectric modules, Hassanniadoon et al. [20] used solar water heaters to transfer heat to the water storage from the surface of the solar heat absorber. To generate thermoelectric power by focusing sunlight, Fresnel lenses were used. Using a radiation intensity of 705.98 W/m^2, the researchers determined that the maximum thermoelectric power is 1.08 W. The thermal efficiency of the system was approximately 51.58 %. Lin et al. [21] studied the temperature and output power of the thermoelectric photovoltaic system for both combined and non-combined modes. After solving their equations using the modified Newton-Raphson method, they discovered that the thermoelectric module, with the photovoltaic cell, reaches a higher temperature than it does in its single state and that the combined system is less efficient than the photovoltaic system in general. Metwally et al. [22] studied a photovoltaic panel cooling model as an active and hybrid cooling system. Thermal generators are used in the active cooling system to dissipate the heat the photovoltaic panels generate. Photovoltaic panels dissipate heat using a thermoelectric generator and phase change material in a hybrid cooling system. They experienced an enhancement in the efficiency of the panel by 2.5 %. Hasheminasab et al. [23] developed and analyzed a theoretical heat transfer model in a thermoelectric thermal photovoltaic hybrid system. For this purpose, they used MATLAB. Their system included a thin aluminum sheet photovoltaic module, a thermoelectric module with aluminum fins to increase the conductivity, and a cool air channel to cool the cold side. This system was analyzed under different radiation conditions, and the result was to determine the optimal number of thermoelectric modules. Also, the total produced power and the efficiency of the combined system were calculated under different radiation conditions. According to their results, a higher amount of radiation leads to a greater temperature difference on the two sides of the thermoelectric and, therefore, a greater thermoelectric output. Nevertheless, a greater radiation intensity reduces the efficiency of the photovoltaic system and increases its temperature, so depending on the existing cooling system, the amount of radiation should be chosen. Under the irradiation of 2800 W/m^2, the combined photovoltaic panel comprised of 36 thermoelectric modules produced 145 W with photovoltaic panels, and the module system produced 4.4 W. In another study [24], the Peltier effect was proposed to dissipate heat from the photovoltaic module. This was accomplished by developing a detailed model and simulating it with MATLAB software to determine the temperatures at different points and calculate how much power is required by thermoelectric cooling modules and photovoltaic cells. Then genetic algorithm optimization is used to accurately determine the thermoelectric supply current so that the whole system's produced power is optimal. Finally, this research showed that the designed system reduced the temperature of the solar cell by consuming a reasonable amount of electrical energy. Also, if the thermoelectric materials are upgraded with higher degrees of efficiency and also higher levels of radiation, the proposed system will perform better. In the hybrid system described [25], solar cells cover a thin silicon film, and thermoelectric generators are used. The thermoelectric generator was also modeled using finite element methods. Photovoltaic cells and thermoelectric generators produce more power due to integrated designs. This system's total production power is 393 mW, twice how much the cell can produce alone. According to Ref. [26], thermoelectric photovoltaic systems can be formed with or without glass. The glass was investigated first and showed that it performs better in conditions of high concentration ratio and increased transmission. In addition, wind speed

was investigated as an important factor, and the nanofluid flow rate was often overlooked in different research. In addition, when thermoelectric efficiency reaches a maximum, electrostatic resistance becomes more optimal than its corresponding value when overall efficiency reaches a maximum. Because nanofluid has a higher thermal conductivity coefficient than water, it shows better results.

A monocrystalline photovoltaic module and a 1000-W halogen lamp were used as light sources in another study by Pang et al. [27] to investigate the combined thermoelectric, photovoltaic system thermal performance. A thermal well behind the thermoelectric module was found to improve the system's thermal performance. Fisac et al. [28] evaluated photovoltaic module performance in two modes with and without thermoelectric generators. This study utilizes thermoelectric generators to optimize photovoltaic module efficiency as temperature increases. Thermovoltaic hybrid systems under concentrated radiation were analyzed numerically [29–36]. Polymer crystalline silicon and thin film silicon cells were studied in their study. Semiconductor equations were used to investigate the effect of temperature on photovoltaic cell efficiency, and it found that polycrystalline thin-layer silicon cells were more suitable for concentrated hybrid systems than polymer cells. Optimizing thermoelectric cooling for active cooling in solar cells was done by Verma et al. [37]. In their research, using the mathematical governing equations of the thermoelectric module and assuming that the properties of the materials used are temperature dependent, the optimal performance of the thermoelectric module was investigated using the method of maximum tracking of the solar rays. The solar cell's electrical efficiency increased by about 1.8 % in this experiment [38].

One of the most important challenges in most of the mentioned hybrid systems is the amount of sunlight reflected from the surface of the photovoltaic cell. By reducing this reflection, more electrical energy can be obtained [39–43]. In comparison to conventional systems, our proposed method offers distinct advantages, particularly in addressing the economic aspect of energy production. By integrating a hybrid system within a specially designed cavity, we mitigate reflective losses from the surfaces of photovoltaic cells, thus enhancing overall efficiency.

Still, from the economic point of view, the cost of energy production is currently higher than common systems. Therefore, in this research, the hybrid system of this cavity system has been used to reduce its reflection from the surfaces of the photovoltaic cell. The proposed model in this research consists of the combination of thermoelectric, photovoltaic module and thermoelectric modules inside a cube as a solar absorber cavity in such a way that the combined system is placed on the lower face of this cube and absorbs the energy of the reflected rays from the surface of the photovoltaic cell. Thermoelectric modules are installed on the side faces. The reflected rays from the bottom surface do not have the appropriate wavelength for production in photovoltaic cells and cause more heating of other surfaces. These cells were removed from the side surface to reduce the price of electricity produced, and only thermoelectric modules were included. One of the advantages of using the absorber cavity is the reduction of reflective losses due to the increase of the apparent absorption coefficient of the mentioned system. This study aims to theoretically investigate the effect of using the cavity on the performance of the combined photovoltaic, thermoelectric system. For this purpose, the governing equations of the problem, including heat transfer and the equations related to photovoltaic and thermoelectric, have been developed numerically.

2. Modeling the combined thermoelectric photovoltaic system

The desired system is according to Fig. 1. The heat transfer process is such that light rays enter the cavity diffused and uniformly in all directions. Electric power is produced when the rays hit the internal surfaces of the absorber, which is the same as the photovoltaic module at the bottom level and the thermoelectric generator at the side surfaces. Then the system's stability increases the temperature of the hot plate of the thermoelectric generator and the photovoltaic module. Additional power can be generated by the thermoelectric generators attached to the photovoltaic module to use this temperature and thermal capability. All three types of heat transfer mechanisms are evident in this combined system. This way, the heat transfer inside the cavity and between its faces is radiation type. Also, heat transfer is conducted in the walls, and considering that the surfaces of the cavity are in contact with air from the inside and outside, convection heat transfer also plays a role in this.

It should be noted that because the incoming radiation includes different wavelengths, not all can produce electrical energy in photovoltaics. Its infrared part only increases the temperature of photovoltaics. In other words, the hot source for thermoelectric modules is the increased temperature of photovoltaics, and the cold source is the outside environment. In this research, T1 shows the temperature of the internal surfaces of the plate cavity, T2 depicts the temperature behind the photovoltaic cell on the bottom, T3 the temperature behind the thermoelectric module on the bottom surface of the cavity, and T4 the temperature behind the thermoelectric module installed on the side. The difference between T2 and T3 at the bottom level is the factor of generating an electric current in thermoelectric generators installed in the hybrid system. The temperature difference between T1 and T4 is the factor of generating an electric current in thermoelectric generators at the surface. On the side, their hot plate is heated by direct radiation. The cavity is in dimensions 110 × 110 mm. The photovoltaic panel is located in the bottom surface of the cavity. Also, TEG panels are situated in the side panels to maximize the power generation in this hybrid system.

2.1. Thermal modeling of the hybrid system

In setting the stage for our solution, we establish several key assumptions that underpin the analysis of our hybrid system. First and foremost, we assume a state of equilibrium, with our hybrid system existing in a steady state throughout our analysis. This foundational assumption provides a stable framework upon which to build our exploration of the system's behavior.

Moving forward, we invoke Kirchhoff's law to simplify our analysis, effectively negating the spectral and angular effects of the photovoltaic module surface. This simplification allows us to treat the absorption and emission coefficients as equal across all wavelengths and directions, streamlining our calculations.

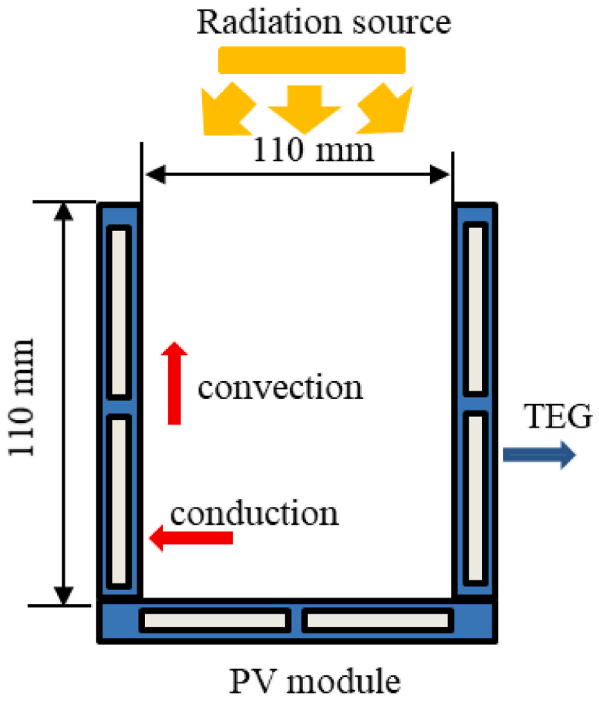

Fig. 1. The schematic view of the cavity.

Furthermore, we presume one-dimensional conduction heat transfer within the photovoltaic panel, extending from the interior to the exterior of the module. This simplifying assumption aids in modeling the thermal behavior of the panel, facilitating a more tractable analysis.

In our modeling, we assume a uniform surface temperature distribution across the photovoltaic module, simplifying the complexity of thermal gradients within the system. This uniformity assumption enables a clearer understanding of the system's overall thermal dynamics.

Moreover, we adopt a diffuse behavior for the photovoltaic module's surface, where both emission intensity and incoming radiation intensity are considered constant in all directions. This simplification enhances the clarity of our analysis by eliminating directional dependencies.

Additionally, we treat the photovoltaic module as having “gray” properties, meaning its characteristics remain consistent across all wavelengths. This assumption allows us to generalize our analysis without the need for wavelength-specific considerations.

Given the ambient air temperature within the cavity falls within normal ranges, we discount its impact on radiation mechanisms, acknowledging only a minimal effect on convection heat transfer.

Furthermore, we assume heat transfer within the thermoelectric generator occurs solely through conduction, with no contribution from radiation. This simplifying assumption facilitates a clearer understanding of the thermoelectric system's operation.

Lastly, we consider a basic photovoltaic module configuration, assuming its economical viability without additional anti-dust or anti-reflection layers on the semiconductor material. This simplification allows us to focus on core system dynamics without delving into secondary considerations.

2.1.1. Radiant heat transfer analysis inside the cavity

Because the air inside the chamber is non-cooperative, the cavity's internal surfaces are opaque (transmission coefficient, zero), and the properties are independent of the wavelength. Diffusivity is assumed in terms of emission and reflection. The net radiation flux of each element inside the cavity and the radiation power entering it can be calculated using the radiosity method (cavity theory) [44].

When analyzing radiation problems using this method, the geometry of the problems should be converted into a completely closed enclosure. However, some levels may not have external existence and are considered virtual. This method assumes that for surfaces with a certain and constant temperature, what amount of flux should be given to or taken from the surface so that the surface remains at the same temperature. The analysis of radiant heat transfer for a closed chamber that has gray and diffuse surfaces is described below. Taking into account the surface energy balance for it, two vectors are introduced into this surface, one of which is the irradiation power ($q_{i,k}A_k$), and the second is the power that must be given to that surface to remain in equilibrium (Q_k) and keep its temperature constant.

On the other hand, the output vector from it is equivalent to the radiation output from the surface, including the reflection of the radiation entering it and the emission from the surface itself, which is known as radiosity ($q_o, k\,A_k$). The equations related to the balance of this level are 1 and 2 [44]:

$$q_{o,k} = \epsilon_k e_{bk} + \rho_k q_{i,k} \tag{1}$$

$$Q_k = \left(q_{o,k} - q_{i,k}\right) A_k \tag{2}$$

ϵ_k is the emission coefficient, ρ_k is the reflection coefficient, and A_k is the area of the k-th surface. According to the radiation heat transfer equations and the approximation of the electric resistance-voltage equations, the Q_k will be in the form of equation (3).

$$Q_k = \frac{e_{bk} - q_{o,k}}{\frac{1-\epsilon_k}{\epsilon_k A_k}} = \frac{\epsilon_k A_k}{1-\epsilon_k}\left(e_{bk} - q_{o,k}\right) \tag{3}$$

After simplification, we will have:

$$\varepsilon_k . b_{bk} = \sum_{j=1}^{N} \left[\delta_{kj} - \left(1-\varepsilon_k\right).F_{k-1}\right].q_{o,j} \tag{4}$$

Therefore, in the chamber, for the surfaces with a known temperature, the boundary condition of constant temperature can be used. With the help of equation (4), the temperature value can be calculated. On the other hand, the heat flux may be constant on some surfaces. In this case, we will use equation (2) and have relevant simplifications.

$$\frac{Q_k}{A_k} = \sum_{j=1}^{N} \left[\delta_{kj} - F_{k-1}\right].q_{o,j} \tag{5}$$

It should be noted that the hybrid cavity has both of the above states, so the combination of two equations, 4 and 5, should be used. The mentioned method is an indirect formulation of the cavity theory method.

In the above matrix, the F is related to the visibility coefficient between the different faces of the absorbent cavity, which was calculated using the Monte Carlo method in this research. If both solar radiation and convective heat flux enter the surfaces at the same time, it will be necessary to correct equation (5) in the form of equation (6) [45]:

$$\frac{Q_k}{A_k} + q_{solar} - q_{convection} = \sum_{j=1}^{N} \left[\delta_{kj} - F_{k-1}\right].q_{o,j} \tag{6}$$

2.1.2. *Investigation of convective heat transfer inside the absorbent cavity*

In previous studies, convective heat transfer has been performed for large cubic cavities in Ref. [46] and for hemispherical and cylindrical cavities in Refs. [47,48]. In order to calculate the convective heat transfer coefficient in this research, the result obtained in Ref. [49] was used. Therefore, equation (7) was considered as Nusselt for the absorbent cavity walls:

$$Nu = \exp\left(-1.736 + 0.34\ \ln\left(Ra_w\right)\right) \tag{7}$$

$$h = \frac{k_{air}}{L} 0.001 . Ra_w^{0.76} \left(\frac{T_s}{T_\infty}\right)^{0.11} \tag{8}$$

Where 2L is the size of the hole opening, K_{air} is the conductivity of the air, and Ra_w is the Rayleigh number. Also:

$$Ra_w = \frac{g.\beta}{\nu.\alpha}\left(T_s - T_\infty\right).L^3 \tag{9}$$

$$\beta = \frac{1}{T} \tag{10}$$

$$\nu = \frac{\mu}{\rho} \tag{11}$$

$$\alpha = \frac{k_{air}}{\rho C_p} \tag{12}$$

And the properties of air can be calculated in the above relationships at the temperature of the air film according to equation (13) [50].

$$k_{air} = \frac{0.000314177 T_{air}^{0.7786}}{1 + \frac{-0.7116}{T_{air}} + \frac{2121.7}{T_{air}^2}} \tag{13}$$

$$\mu_{air} = \frac{1.425 \times 10^{-6}.T_{air}^{B}}{1 + \frac{108.3}{T_{air}}} \tag{14}$$

$$\rho_{air} = \frac{P_{air}}{RT_{air}} \tag{15}$$

$$C_p = 1100\frac{kJ}{kg.K} \tag{16}$$

which is R = 287.05 $\frac{J}{kg.K}$, and P_{air} is the air pressure. Finally, when considering the temperature of the surfaces, the value of the convective heat transfer coefficient was calculated. The amount of convection heat transfer flux from the walls can be calculated according to equation (17):

$$q_{conv} = h.\left(T_{avg-surface} - T_{film}\right) \tag{17}$$

2.1.3. Calculating the power of photovoltaic cell and thermoelectric generator

Equations (18) and (19) are used to calculate the photovoltaic cell's short-circuit current and open-circuit voltage [51,52].

$$I_{sc} = I_{sc-ref}\frac{G}{G_{ref}}\left(1 + K_l\Delta T\right) \tag{18}$$

$$V_{oc} = V_{oc-ref}\left(1 + K_V\Delta T\right) \tag{19}$$

In these equations, I_{sc-ref} and V_{oc-ref} are short circuits current and open circuit voltage under standard test conditions (radiation intensity of 1000 W/m^2 and temperature of 25 °C. ΔT is the temperature difference value compared to the standard test temperature. A manufacturer must also calculate the short-circuit current and open-circuit voltage temperature coefficients. Usually, for monocrystalline silicon cells, K_V is about 0.5 VK^{-1}, but as in many types of research in the field of thermoelectrics, such as [53], thermoelectric generators are considered open circuits, and it is necessary to express the equation related to the maximum power that can be extracted from the generator (when the internal resistance is equal to the external resistance of the load).

$$P_{max} = \frac{1}{4}\frac{\left(V_{oc}\right)^2}{R_i} \tag{20}$$

R_i is the internal electrical resistance of the thermoelectric generator that is determined by its manufacturer. Also, the open circuit voltage from Equation (21) is the coefficient of the module. It will be obtained.

$$V_{oc} = S.\left(T_h - T_c\right) \tag{21}$$

Also, the optimal flow is in the form of equation (22).

$$I_{teg} = \frac{S\left(T_h - T_c\right)}{2T_m} \tag{22}$$

where $T_m = T_h + T_c/2$.

2.2. Problem-solving algorithm

A different solution method has been proposed to solve the problem because the proposed system is hybrid and utilizes photovoltaic and thermoelectric technology. This solution method has been implemented in MATLAB. The flux entering each surface is known and equal to zero because all surfaces are insulated. Due to its virtual nature and the direct impact of solar flux on the lower surface, the upper surface (opening) is at absolute zero. The surface temperature, thermal conductivity, reflection, and convection heat transfer are calculated in each step. The problem continues until the energy balance is within 0.001 % of the error.

$$\left|\frac{Q_{solar} - Q_{reradiation} - Q_{convection} - Q_{conduction} - Q_{radiation,out}}{Q_{solar}}\right| \leq 10^{-3} \tag{23}$$

2.3. Specifications of photovoltaic module and thermoelectric module

The specifications of the used converters and photovoltaic modules in the present study are presented in Table 1.

T1-T4 represent temperature values at different points within the system, crucial for assessing temperature differentials essential for power generation in thermoelectric generators. Additionally, the convective heat transfer coefficient (h) and Rayleigh number (Ra_w) are pivotal in determining heat transfer rates within the cavity.

Table 1
Thermoelectric module and photovoltaic cell specifications.

Parameter	Value for thermoelectric module	Values for photovoltaic cell
Width (mm)	40	110
Length (mm)	40	110
Height (mm)	4.8	5
Maximum voltage (V)	3.6	5.8
Maximum current (A)	1.23	160
Maximum electrical power (W)	4.5	0.92
Efficiency (%)	5.4	9.8
Resistance (Ω)	3	–
Thermal resistance (K/W)	2.6	–
Open circuit current (mA)	–	177
Open circuit voltage (V)	–	6

3. Results and discussion

The cavity studied in this research consists of a thermoelectric, photovoltaic hybrid on the bottom of the cube and 20 thermoelectric generators on the side surfaces, which are exposed to radiation or different power levels. The equations of radiation and convection heat transfer inside the cavity, thermal conduction from the walls, and electric power equations are solved numerically. At first, to validate the performance of the numerical solution, the governing equations were solved assuming all hybrid surfaces. The results obtained with the values obtained from the experimental work of Farhangian et al. [38] were compared. In the experimental sample, the entire surface of the cavity was made of the hybrid system so that all the internal faces of the cube were made of photovoltaic cells. This sample has been tested in the laboratory against the simulated radiation of the metal halide lamp and also against the sunlight in real conditions [38].

The results of the numerical solution for a cavity with all hybrid surfaces are shown with the experimental results in Fig. 2. Comparing the temperature and power values shows that the difference between the numerical solution and the experimental results is less than 8 %. Most of these differences are due to the assumptions of the numerical solution.

Fig. 3 indicates the temperature changes behind the thermoelectric module installed on the side surfaces under irradiation of 1000 W/m^2 under different convective heat transfer coefficients outside the cavity. The higher the HTC, the lower the photovoltaic cell temperature, which is more suitable for increasing efficiency. According to Fig. 3, in very low amounts of convective heat transfer, only heat conduction occurs with the surrounding environment, and the photovoltaic cell temperature reaches 69 °C.

As shown in Fig. 4, the photovoltaic cell temperature increases with radiation entering the cavity. This heat is conducted to the external surfaces, which increases the temperature of the thermoelectric hot plate.

The temperature difference between the inner surface of the photovoltaic cell and the hot and cold plate of the thermoelectric generator exists at any amount of radiation, increasing with the input radiation. Using equations (20) and (21) and the temperature difference between the hot and cold plate of the thermoelectric generator, which is illustrated in Fig. 4, the amount of produced power by the thermoelectric generators on the side surfaces and the thermoelectric generator installed in the hybrid system is calculated at the bottom surface. In different heat transfer coefficients of the surrounding environment, as shown in Fig. 5, with the increase in this parameter, the temperature difference between the hot and cold plate increases, and therefore the amount of production power is at its maximum at the heat transfer coefficient of 10 W/m^2K, and it reaches 352.48 mW. Although doubling the convective coefficient is

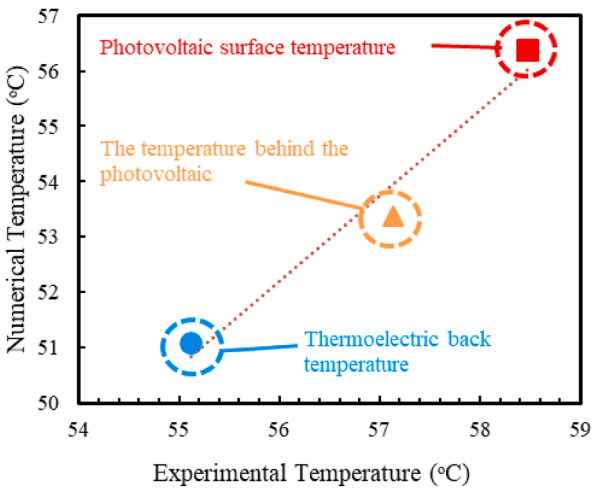

Fig. 2. The validation of simulations with the experimental results of [38].

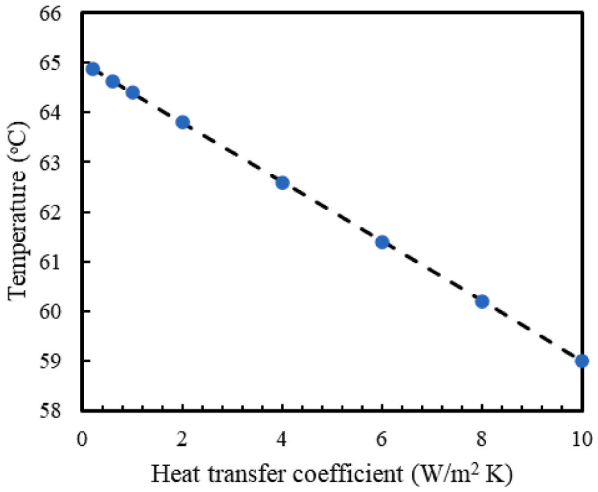

Fig. 3. The variations of photovoltaic cells in different heat transfer coefficient.

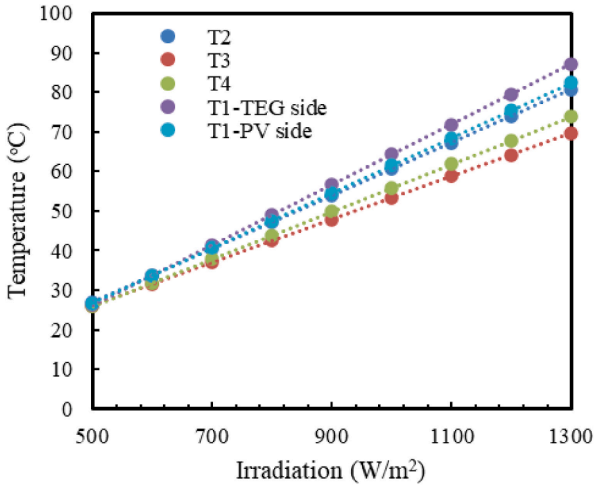

Fig. 4. The variation of surface temperature with different irradiation.

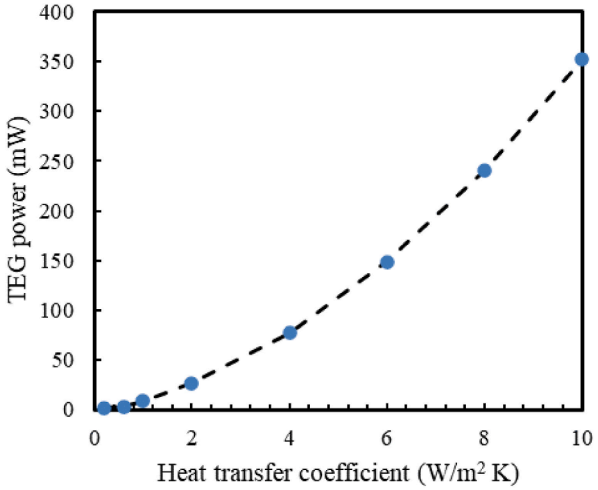

Fig. 5. The TEG power with various heat transfer coefficients at irradiation of 1000 W/m^2.

associated with cost, and its provision is not so easy in the points where solar energy is used, it results in a threefold increase in power production. In addition, cooling the photovoltaic cell surface effectively increases efficiency and reduces cell damage. As radiation intensity increases, more energy is absorbed by the PV cell, leading to an elevation in its temperature. This rise in temperature creates a greater temperature differential between the PV cell and the surrounding environment. Simultaneously, the TEG absorbs heat from the hot plate and dissipates it through the cold plate, generating electrical power due to the Seebeck effect.

It is highly effective to cool the cold plate to increase the hybrid system's efficiency. Figs. 6 and 7 depict heat convection's effect on the cavity's power generation. While the cavity has the photovoltaic plate at its bottom, the cooling behind the thermoelectric cold plate on its side surfaces, as well as its bottom surface, is similar, and due to the significant increase in the amount of power production, it may be used in a variety of applications and will increase heat transfer coefficients. In a thermoelectric module, electrical current is generated when there is a temperature gradient across the module, known as the Seebeck effect. The cold side of the TEG serves as a sink for heat dissipation, ensuring that there is a significant temperature difference between the hot and cold sides of the module. By cooling the cold plate, the system maintains a lower temperature on this side, which effectively widens the temperature gradient across the TEG.

The thermoelectric generator's main power source depends on the temperature difference, as illustrated in Fig. 7. The output power increases six times because of doubling the heat transfer coefficient. Fig. 8 shows the total power output of the cavity. It can be seen that the thermoelectric generator's temperature difference increases with an increase in the HTC. As a result, the photovoltaic cell and thermoelectric generator produce more power while cooling the photovoltaic plate. The Seebeck effect states that a voltage difference is generated across a thermoelectric material when there is a temperature gradient applied to it. In the context of the hybrid system, the thermoelectric modules experience a temperature difference between the hot and cold sides, which drives the flow of electrical current and thus power generation.

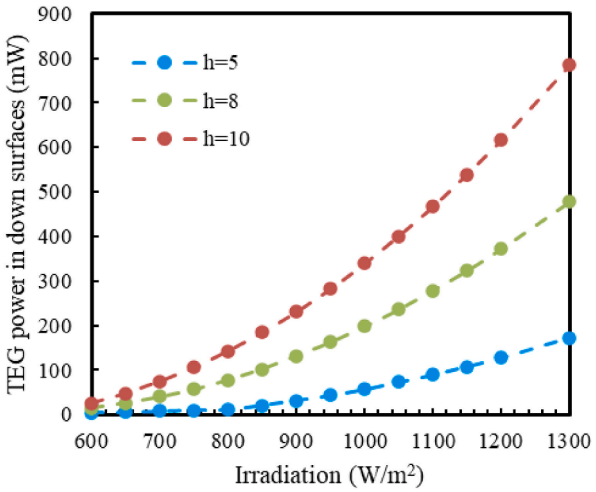

Fig. 6. The TEG power generation in the down surface with various heat transfer coefficients and different irradiations.

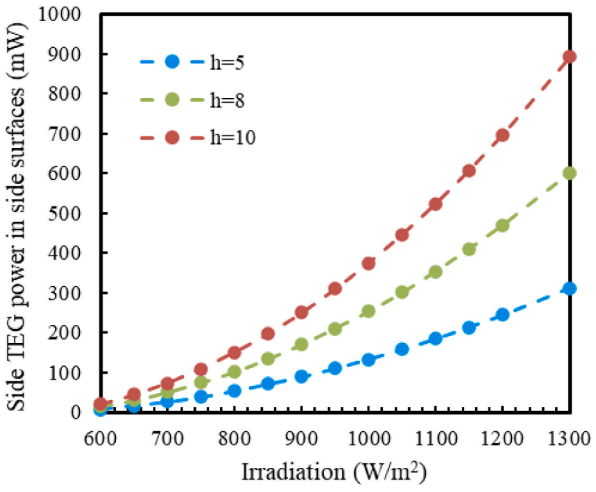

Fig. 7. The TEG power generation in the side surfaces with various heat transfer coefficients and different irradiations.

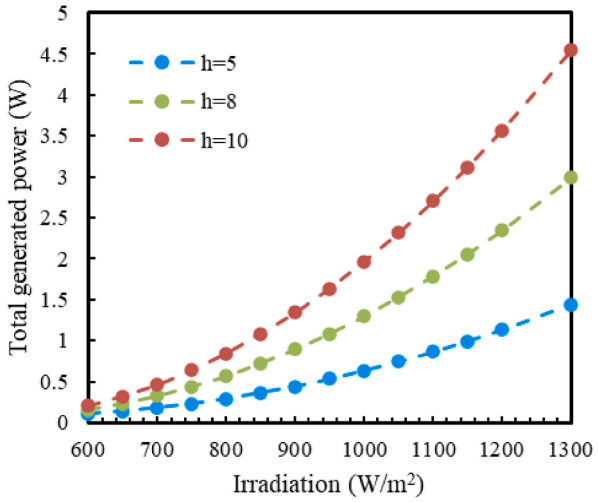

Fig. 8. The total generated power under various irradiation.

The comparison of the numerical and the experimental results in the irradiation of 1000 W/m^2 is presented in Fig. 9. It is observed that in the range of 5 W/m^2K, the use of thermoelectric modules in the side wall instead of photovoltaic cells increases the amount of electric current generation by 1.4 times. With this method, the cost of constructing the absorbent cavity can be reduced in addition to increasing the power. In fact, solving the distribution of radiation on different surfaces of the cavity shows that the amount of direct radiation energy that reaches the bottom surface of the cavity is approximately 1.7 times in the condition that the incoming radiation is perpendicular to the opening of the cavity. This distribution is given in Table 2. A comparison of the results in Table 2 shows that 30 % of the radiation energy directly hits the bottom surface of the cavity, and only 10 % of the incoming radiation is reflected in the surrounding environment.

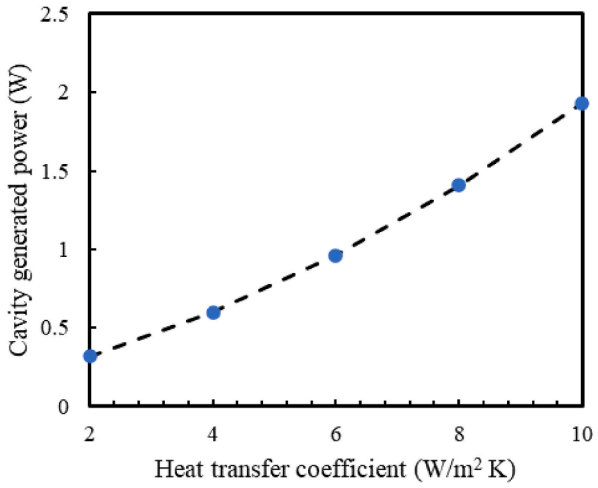

Fig. 9. The comparison of the total cavity generated power using the simulation with different heat transfer coefficients.

Table 2
The distribution percentage of irradiation on the cavity.

The component	Irradiation distribution
TEG side 2	15 %
TEG side 3	15 %
TEG side 4	15 %
TEG side 5	15 %
PV-down side	30 %
Re-radiation	10 %

3.1. Optimizing the dimensions of the hole opening

Decreasing the size of the cavity opening reduces the amount of radiant power entering the cavity, and therefore the output power of the cavity decreases. Still, on the other hand, reducing the amount of wasted reflection increases the system's efficiency. To obtain the optimal size of the hole opening, first, the very important parameter of absorption efficiency of the cavity is checked. The cavity absorption efficiency is calculated from equation (24) [54].

$$\eta_{abs} = \frac{\alpha_{eff} P_{aperture} - \epsilon_{eff} A_{aperture} T^4}{Q_{solar}} \tag{24}$$

where α_{eff} and ϵ_{eff} are the absorption and scattering coefficients of the cavity, respectively. $P_{Aperture}$ is the amount of radiant power entering the cavity opening. Another important parameter for checking the effect of the opening is the opening ratio parameter. This is obtained from the ratio of the size of the opening area to the size of the hole's surface area. Fig. 10 shows the graph of the highest absorption efficiency in aperture opening ratio in different radiations. As shown in the figure, the absorption efficiency reaches its maximum value in the opening ratio of 0.43, i.e., 96.5 %.

3.2. Economic analysis

Levelized cost of energy (LCOE) is a method based on calculating the current value of the investment and operation costs of electricity production throughout the entire life of the project [55]. LCOE can be calculated from equation (25) [56].

$$LOCE = \frac{\sum_{t=0}^{N} \left(\frac{(I_t + O_t + M_t)}{(1+r)^t} \right)}{\sum_{t=0}^{T} \left(\frac{P_t (1-d)^d}{(1+r)^t} \right)} \tag{25}$$

In which N is the lifetime of the project, I_t is the investment cost of the project, including construction cost, operation cost, maintenance cost, P_t is the annual energy production rate in terms of (kWh/year), d is the annual degradation rate (%), and r is the discount rate (%).

In this research, the I_t for the proposed hybrid system is $82.75 based on the price of the laboratory sample, which is based on the discount rate, the production degradation rate of 5 %, the repair and operation rate of 7.5 %, the annual investment rate, and the lifespan of 30 years. The LCOE is equal to 6.78 $/kWh. The LCOE rate for a photovoltaic cell is 0.92, and for a hybrid flat plate consisting of a photovoltaic cell and four thermoelectric generators is 5.65 [56]. Research [57,58] shows that the price of current thermoelectric generators decreases with the increase in the number of industrial scales to the extent of photovoltaic cells; therefore, their use is economical. Of course, with the growth of technology in constructing thermoelectric generators with a higher degree of competence, the production power would increase against the lower temperature difference. Therefore, the cost of electricity will be decreased.

4. Artificial neural networks

In order to propose predictive models, the results of the simulations are used to train artificial neural networks. The models benefit from hyperparameter tuning to better predict the results. Using machine learning algorithms in heat transfer problems is becoming prevalent [59–63]. The models are later evaluated using a testing dataset. It should be noted that the testing dataset is not utilized in the training process [64–68]. The final models of the output parameters are presented in Table 3.

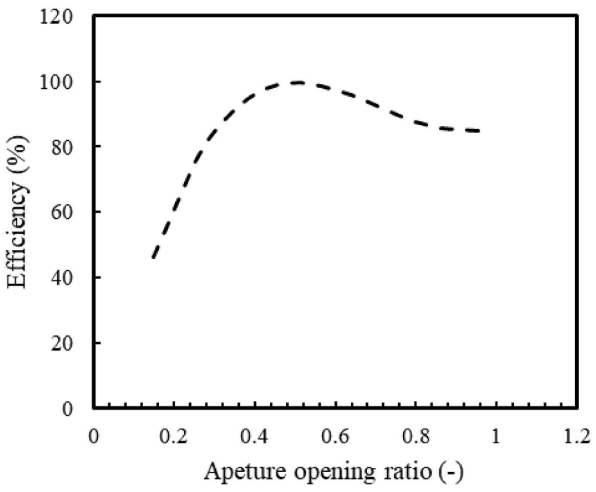

Fig. 10. The variation of efficiency with the changes in aperture opening ratio.

Table 3
The ANN settings for final models.

Hyperparameter	Down surface	Side surface	Total
Layers' structure	(32,64,128,256,128,64,32)	(32,64,128,128,64,32)	(32,64,128,64,32)
Batch size	16	32	16
Epochs	35,000	45,000	25,000
Activation function	Sigmoid	ReLU	ReLU

The results of the model for the generated power in the down and side surfaces are presented in Figs. 11 and 12. It is clear that the model has a sophisticated hidden layer structure, and the model's evaluation shows its accuracy. The model's mean absolute error is equal to 1.01 %.

The model for side surfaces shows that the model error is equal to 1.68 %, and the model has R^2 of 0.98. This shows the accuracy of the model.

The best model is depicted in Fig. 13, and it predicts total generated power. It is clear that the accuracy of this model is very satisfactory since it has an MAE of 0.78, and the R^2 is 0.99.

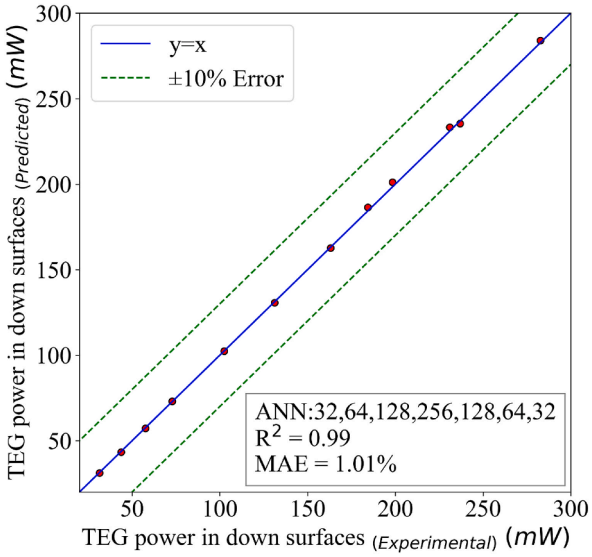

Fig. 11. The artificial neural network prediction of the generated power in the down surface.

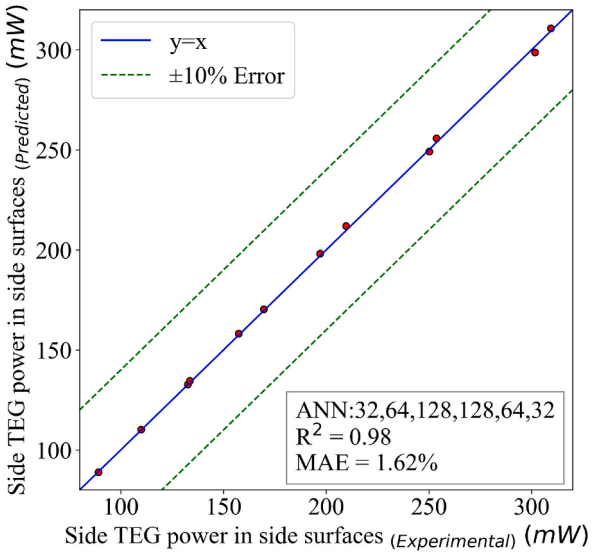

Fig. 12. The artificial neural network prediction of the generated power in the side surfaces.

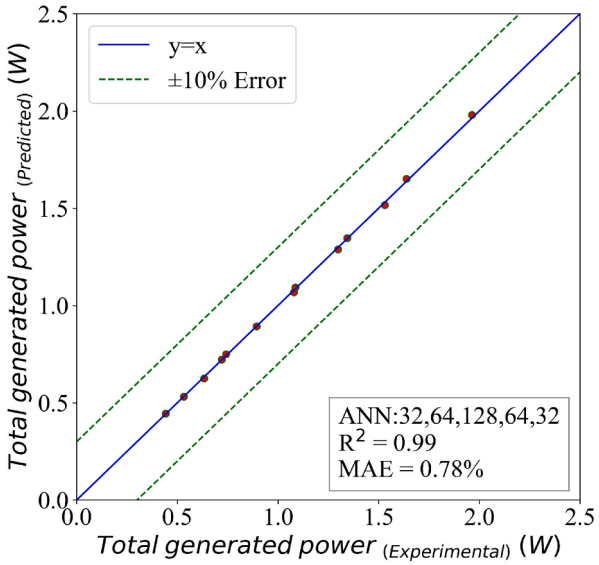

Fig. 13. The artificial neural network prediction of the total generated power in the cavity.

4.1. Machine learning algorithm dissemination

To increase the model's novelty and challenge the proposed models, the results of other experiments [38] are compared with the predictions of the current study. The results are satisfactory, and the models could replace time-consuming experiments and simulations [69]. A similar study is presented in many research [70–73]. Fig. 14 shows the result of the produced power on the side surface. The results show an MAE of 4 % and the R^2 is 0.95.

A similar analysis has also been done for the bottom surface, which is presented in Fig. 15. The model predicts the experimental results of [38] on the bottom surface. It is concluded that the proposed model of the present study has 3 % MAE and the R^2 is 0.97. The results show how machine learning algorithms are able to capture the physics of the hybrid system and can predict the results accurately.

5. Conclusion

In conclusion, this research introduces a novel model of a combined thermoelectric-photovoltaic system, leveraging an absorption cavity structure to enhance efficiency by absorbing reflected solar radiation from the photovoltaic cell in multiple directions. We have established that the optimal placement for the hybrid system is at the cavity's bottom, where the highest concentration of incoming

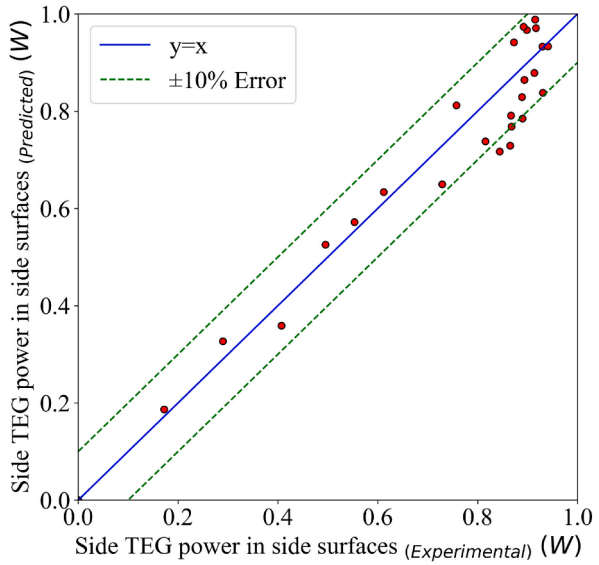

Fig. 14. The ANN prediction of produced power in side surfaces using experimental results of [38].

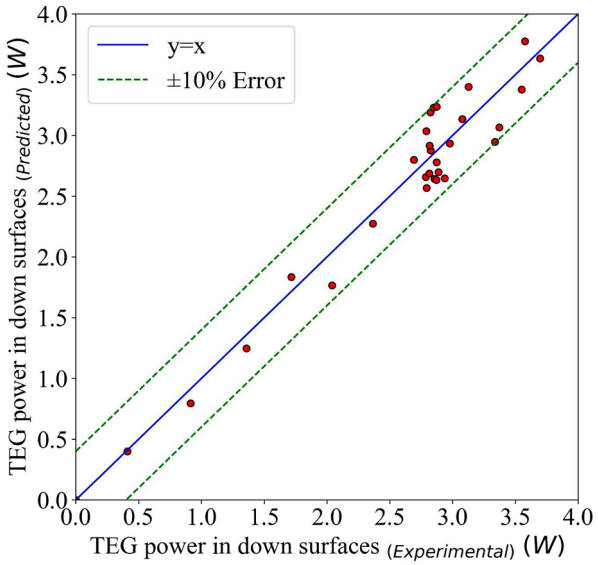

Fig. 15. The ANN prediction of produced power in the bottom surface using experimental results of [38].

radiation, approximately 30 %, is observed. Heat transfer analysis indicates a significant reduction in reflection from the cavity opening, from approximately 10 % with the opening to 60 % without it. Moreover, experimentation with various external heat transfer coefficients demonstrates a direct correlation between coefficient increase and enhanced power generation, attributed to decreased cold side temperatures and improved photovoltaic cell performance. Notably, the system's design accounts for the diverse wavelengths of incoming radiation, with infrared wavelengths primarily contributing to photovoltaic cell heating rather than electricity production. Analysis further reveals that the cavity's maximum solar energy absorption efficiency occurs at an opening ratio of 0.43, reaching 96.5 %. Despite variations in solar tracking, the system exhibits sufficient power generation potential, with a current electricity price of $6.77 per kWh. Additionally, the implementation of artificial neural network models based on simulation results showcases remarkable predictive accuracy, validated through comparison with experimental data. Future research avenues may explore the application of diverse machine learning algorithms for predictive modeling and conduct comparative analyses against alternative experimental findings, further advancing the understanding and optimization of complex solar energy systems.

Funding

This research was funded by the Deanship of Scientific Research at King Khalid University under grant number RGP.2/34/44.

CRediT authorship contribution statement

Haitham Osman: Conceptualization, Methodology, Writing – review & editing. **Loke Kok Foong:** Project administration, Supervision, Writing – original draft. **Binh Nguyen Le:** Data curation, Software, Writing – original draft. **Velibor Spalevic:** Formal analysis, Investigation. **Branislav Dudic:** Formal analysis, Project administration, Writing – review & editing. **Goran Skataric:** Formal analysis, Writing – review & editing.

Declaration of competing interest

The authors declare that they have no known competing financial interests or personal relationships that could have appeared to influence the work reported in this paper.

Data availability

Data will be made available on request.

Acknowledgments

The authors extend their appreciation to the Deanship of Scientific Research at King Khalid University for funding this work through Research Groups Program under grant number RGP.2/34/44.

References

[1] J. Hu, Y. Zou, N. Soltanov, A multilevel optimization approach for daily scheduling of combined heat and power units with integrated electrical and thermal storage, Expert Syst. Appl. (2024) 123729.
[2] B. Jalili, A. Shateri, A. Akgül, A. Bariq, Z. Asadi, P. Jalili, D.D. Ganji, An investigation into a semi-porous channel's forced convection of nano fluid in the

presence of a magnetic field as a result of heat radiation, Sci. Rep. 13 (1) (2023) 18505.
[3] M. Hou, Y. Zhao, X. Ge, Optimal scheduling of the plug-in electric vehicles aggregator energy and regulation services based on grid to vehicle, Int. Trans. Electr. Energy Syst. 27 (6) (2017) e2364.
[4] M. Dehghan Afifi, B. Jalili, A. Mirzaei, P. Jalili, D. Ganji, The effects of thermal radiation, thermal conductivity, and variable viscosity on ferrofluid in porous medium under magnetic field, World J. Eng. (2024).
[5] G. Liu, Data collection in MI-assisted wireless powered underground sensor networks: directions, recent advances, and challenges, IEEE Commun. Mag. 59 (4) (2021) 132–138.
[6] P. Jalili, A.A. Azar, B. Jalili, D.D. Ganji, Study of nonlinear radiative heat transfer with magnetic field for non-Newtonian Casson fluid flow in a porous medium, Results Phys. 48 (2023) 106371.
[7] A. Jafaripournimchahi, A. Shateri, B. Jalili, P. Jalili, D.D. Ganji, The effects of magnetic field and thermal radiation on the mixed convection of Al2O3-Cu/water hybrid nanofluid over a permeable vertical flat plate, Mod. Phys. Lett. B (2024) 2450242.
[8] P. Sundarraj, D. Maity, S.S. Roy, R.A. Taylor, Recent advances in thermoelectric materials and solar thermoelectric generators–a critical review, RSC Adv. 4 (87) (2014) 46860–46874.
[9] J. Zhang, Y. Chen, Y. Gao, Z. Wang, G. Peng, Cascade ADRC speed control base on fcs-mpc for permanent magnet synchronous motor, J. Circ. Syst. Comput. 30 (11) (2021) 2150202.
[10] J. Gao, Y. Zhang, X. Li, X. Zhou, Z.J. Kilburn, Thermodynamic and thermoeconomic analysis and optimization of a renewable-based hybrid system for power, hydrogen, and freshwater production, Energy (2024) 131002.
[11] S. Li, X. Fang, J. Liao, M. Ghadamyari, M. Khayatnezhad, N. Ghadimi, Evaluating the efficiency of CCHP systems in Xinjiang Uygur Autonomous Region: an optimal strategy based on improved mother optimization algorithm, Case Stud. Therm. Eng. 54 (2024) 104005.
[12] H. Alimoradi, M. Shams, N. Ashgriz, Bubble behavior and nucleation site density in subcooled flow boiling using a novel method for simulating the microstructure of surface roughness, Kor. J. Chem. Eng. 39 (11) (2022) 2945–2958.
[13] M. Fei, Z. Zhang, W. Zhao, P. Zhang, Z. Xing, Optimal power distribution control in modular power architecture using hydraulic free piston engines, Appl. Energy 358 (2024) 122540.
[14] K.S. Qananba, M.D.A. Al-Nimr, Utilizing the wasted heat from the secondary reflector of linear fresnel solar system by installing thermoelectric generator modules and reheating the working fluid, Arabian J. Sci. Eng. (2023) 1–19.
[15] B. Jalili, A. Rezaeian, P. Jalili, D.D. Ganji, Y. Khan, Squeezing flow of Casson fluid between two circular plates under the impact of solar radiation, ZAMM-J. Appl. Math. Mech. Z. Angew. Math. Mech. 103 (9) (2023) e202200455.
[16] B. Jalili, M. Emad, P. Jalili, D.D. Ganji, S. Saleem, E.M. Tag-eldin, Thermal analysis of boundary layer nanofluid flow over the movable plate with internal heat generation, radiation, and viscous dissipation, Case Stud. Therm. Eng. 49 (2023) 103203.
[17] Y. Li, S. Witharana, H. Cao, M. Lasfargues, Y. Huang, Y. Ding, Wide spectrum solar energy harvesting through an integrated photovoltaic and thermoelectric system, Particuology 15 (2014) 39–44.
[18] H. Alimoradi, M. Shams, Numerical simulation of the effects of surface roughness on nucleation site density of nanofluid boiling, Modares Mech. Eng. 19 (7) (2019) 1613–1622.
[19] A. Faddouli, M. Hajji, S. Fadili, B. Hartiti, H. Labrim, A. Habchi, A comprehensive review of solar, thermal, photovoltaic, and thermoelectric hybrid systems for heating and power generation, Int. J. Green Energy (2023) 1–35.
[20] M. Hassasnniadoon, A. Abbaszadeh, A. Moazemighodarzi, "Experimental Investigation of fresnel lens application in a solar water heater with the electricity generation via thermoelectric module, J. Solid. Fluid Mech. 4 (3) (2014) 159–169.
[21] W. Lin, T.M. Shih, J.C. Zheng, Y. Zhang, J. Chen, Coupling of temperatures and power outputs in hybrid photovoltaic and thermoelectric modules, Int. J. Heat Mass Tran. 74 (2014) 121–127.
[22] H. Metwally, N.A. Mahmoud, M. Ezzat, W. Aboelsoud, Numerical Investigation of photovoltaic hybrid cooling system performance using the thermoelectric generator and RT25 Phase change material, J. Energy Storage 42 (2021) 103031.
[23] M. Hasheminasab, A. Bozorgnezhad, M. Shams, G. Ahmadi, H. Kanani, Simultaneous investigation of PEMFC performance and water content at different flow rates and relative humidities, in: International Conference on Nanochannels, Microchannels, and Minichannels, vol. 46278, American Society of Mechanical Engineers, 2014, August V001T07A002.
[24] A. Bozorgnezhad, M. Shams, G. Ahmadi, H. Kanani, M. Hasheminasab, The experimental study of water accumulation in PEMFC cathode channel, in: Fluids Engineering Division Summer Meeting, vol. 57212, American Society of Mechanical Engineers, 2015, July V001T22A004.
[25] A. Bozorgnezhad, M. Shams, H. Kanani, M.R. Hashemi Nasab, Experimental study of the effect of inlet flow parameters on the operation of PEMFC, Modares Mech. Eng. 14 (5) (2014) 33–43.
[26] H. Alimoradi, M. Shams, N. Ashgriz, A. Bozorgnezhad, A novel scheme for simulating the effect of microstructure surface roughness on the heat transfer characteristics of subcooled flow boiling, Case Stud. Therm. Eng. 24 (2021) 100829.
[27] W. Pang, Y. Liu, S. Shao, X. Gao, Empirical study on thermal performance through separating impacts from a hybrid PV/TE system design integrating heat sink, Int. Commun. Heat Mass Tran. 60 (2015) 9–12.
[28] M. Fisac, F.X. Villasevil, A.M. López, High-efficiency photovoltaic technology including thermoelectric generation, J. Power Sources 252 (2014) 264–269.
[29] Y. Deng, W. Zhu, Y. Wang, Y. Shi, Enhanced performance of solar-driven photovoltaic–thermoelectric hybrid system in an integrated design, Sol. Energy 88 (2013) 182–191.
[30] A. Bozorgnezhad, M. Shams, H. Kanani, M. Hasheminasab, Experimental investigation on dispersion of water droplets in the single-serpentine channel of a PEM fuel cell, J. Dispersion Sci. Technol. 36 (8) (2015) 1190–1197.
[31] L. Anbazhagan, P. Sudhanya, R. Jansi, Characteristics analysis of different photonic crystal fiber lattice structures, J. Opt. Photon. Res. (2023).
[32] M. Ashrafi, M. Shams, A. Bozorgnezhad, G. Ahmadi, Simulation and experimental validation of droplet dynamics in microchannels of PEM fuel cells, Heat Mass Tran. 52 (2016) 2671–2686.
[33] A. Bozorgnezhad, M. Shams, H. Kanani, M. Hasheminasab, G. Ahmadi, Two-phase flow and droplet behavior in microchannels of PEM fuel cell, Int. J. Hydrogen Energy 41 (42) (2016) 19164–19181.
[34] A. Bozorgnezhad, M. Shams, H. Kanani, M. Hasheminasab, G. Ahmadi, The experimental study of water management in the cathode channel of single-serpentine transparent proton exchange membrane fuel cell by direct visualization, Int. J. Hydrogen Energy 40 (6) (2015) 2808–2832.
[35] Y.Y. Wu, S.Y. Wu, L. Xiao, Performance analysis of photovoltaic–thermoelectric hybrid system with and without glass cover, Energy Convers. Manag. 93 (2015) 151–159.
[36] J. Zhang, Y. Xuan, L. Yang, Performance estimation of photovoltaic–thermoelectric hybrid systems, Energy 78 (2014) 895–903.
[37] V. Verma, A. Kane, B. Singh, Complementary performance enhancement of PV energy system through thermoelectric generation, Renew. Sustain. Energy Rev. 58 (2016) 1017–1026.
[38] O.F. Marandi, M. Ameri, B. Adelshahian, The experimental Investigation of a hybrid photovoltaic-thermoelectric power generator solar cavity-receiver, Sol. Energy 161 (2018) 38–46.
[39] Y. Wang, J. Xu, L. Qiao, Y. Zhang, J. Bai, Improved amplification factor transport transition model for transonic boundary layers, AIAA J. 61 (9) (2023) 3866–3882.
[40] X. Bai, M. Xu, Q. Li, L. Yu, Trajectory-battery integrated design and its application to orbital maneuvers with electric pump-fed engines, Adv. Space Res. 70 (3) (2022) 825–841.
[41] Y. Kondo, H. Yamashita, Theoretical analysis of thermal radiative equilibrium via a radiosity method, Heat Tran. Asian Res. 41 (8) (2012) 719–732.
[42] M.F. Modest, S. Mazumder, M.F. Modest, S. Mazumder, Fundamentals of thermal radiation, Radiat. Heat Tran. 1 (2003) 1–29.
[43] W. Lipiński, E. Abbasi-Shavazi, J. Chen, J. Coventry, M. Hangi, S. Iyer, A. Kumar, L. Li, S. Li, J. Pye, J.F. Torres, Progress in heat transfer research for high-temperature solar thermal applications, Appl. Therm. Eng. 184 (2021) 116137.
[44] U. Leibfried, J. Ortjohann, Convective Heat Loss from Upward and Downward-Facing Cavity Solar Receivers: Measurements and Calculations, 1995.

[45] J. Zhang, J.Y. Li, T. Wang, Z.S. Qian, Influence of nozzle structure on the flow field of the prestage of nozzle flapper servo valve, Int. J. Hydromechatronics 6 (1) (2023) 59–75.
[46] Y. Yang, Z. Si, L. Jia, P. Wang, L. Huang, Y. Zhang, C. Ji, Whether rural rooftop photovoltaics can effectively fight the power consumption conflicts at the regional scale–A case study of Jiangsu Province, Energy Build. 306 (2024) 113921.
[47] J. Zhang, D. Zhu, W. Jian, W. Hu, G. Peng, Y. Chen, Z. Wang, Fractional order complementary non-singular terminal sliding mode control of PMSM based on neural network, Int. J. Automot. Technol. (2024) 1–12.
[48] S. Li, X. Zhao, W. Liang, M.T. Hossain, Z. Zhang, A fast and accurate calculation method of line breaking power flow based on Taylor expansion, Front. Energy Res. 10 (2022) 943946.
[49] S. Wang, C. Zheng, T. Ma, T. Wang, S. Gao, Q. Dai, Q. Han, F. Chu, Tooth backlash inspired comb-shaped single-electrode triboelectric nanogenerator for self-powered condition monitoring of gear transmission n, Nano Energy (2024) 109429.
[50] D. Qin, X. Wu, J. Zhang, X. Wang, N. Yan, Hydraulic optimisation design of axial flow pump based on blade velocity distribution, Int. J. Hydromechatronics 6 (4) (2023) 311–324.
[51] H. Abdellatif, M.I. Hossain, M.A. Abido, Parameters estimation of PV models using artificial neural network, Arabian J. Sci. Eng. (2022) 1–10.
[52] M. Hou, Y. Zhao, X. Ge, Optimal scheduling of the plug-in electric vehicles aggregator energy and regulation services based on grid to vehicle, Int. Trans. Electr. Energy Syst. 27 (6) (2017) e2364.
[53] S. Choudhuri, S. Adeniye, A. Sen, Distribution alignment using complement entropy objective and adaptive consensus-based label refinement for partial domain adaptation, Artif. Intell. Appl 1 (1) (2023, January) 43–51.
[54] H. Gaur, B. Khidhir, R.K. Manchiryal, Solution of structural mechanic's problems by machine learning, Int. J. Hydromechatronics 5 (1) (2022) 22–43.
[55] Y. Yang, Z. Si, L. Jia, P. Wang, L. Huang, Y. Zhang, C. Ji, Whether rural rooftop photovoltaics can effectively fight the power consumption conflicts at the regional scale–A case study of Jiangsu Province, Energy Build. 306 (2024) 113921.
[56] J. Fan, X. Zhou, Optimization of a hybrid solar/wind/storage system with bio-generator for a household by emerging metaheuristic optimization algorithm, J. Energy Storage 73 (2023) 108967.
[57] C. Yang, T.U.K. Nutakki, M.A. Alghassab, S. Alkhalaf, F. Alturise, F.S. Alharbi, Y. Elmasry, S. Abdullaev, Optimized integration of solar energy and liquefied natural gas regasification for sustainable urban development: dynamic modeling, data-driven optimization, and case study, J. Clean. Prod. (2024) 141405.
[58] Z. Ma, J. Zhao, L. Yu, M. Yan, L. Liang, X. Wu, M. Xu, W. Wang, S. Yan, A review of energy supply for biomachine hybrid robots, Cyborg Bionic Syst. 4 (2023) 53.
[59] M.M. Samy, H.H. Sarhan, S. Barakat, S.A. Al-Ghamdi, A hybrid pv-biomass generation based micro-grid for the irrigation system of a major land reclamation project in kingdom of Saudi Arabia (ksa)-case study of albaha area, in: 2018 IEEE International Conference on Environment and Electrical Engineering and 2018 IEEE Industrial and Commercial Power Systems Europe (EEEIC/I&CPS Europe), IEEE, 2018, June, pp. 1–8.
[60] M. Yang, Y. Wang, X. Xiao, Y. Li, A robust damping control for virtual synchronous generators based on energy reshaping, IEEE Trans. Energy Convers. (2023).
[61] H. Alimoradi, M. Shams, Z. Valizadeh, The effects of nanoparticles in the subcooled boiling flow in the channels with different cross-sectional area and same hydraulic diameter, Modares Mech. Eng. 16 (12) (2017) 545–554.
[62] E. Eskandari, H. Alimoradi, M. Pourbagian, M. Shams, Numerical Investigation and deep learning-based prediction of heat transfer characteristics and bubble dynamics of subcooled flow boiling in a vertical tube, Kor. J. Chem. Eng. 39 (12) (2022) 3227–3245.
[63] K. Gairaa, A. Khellaf, Y. Messlem, F. Chellali, Estimation of the daily global solar radiation based on Box–Jenkins and ANN models: a combined approach, Renew. Sustain. Energy Rev. 57 (2016) 238–249.
[64] P. Li, J. Hu, L. Qiu, Y. Zhao, B.K. Ghosh, A distributed economic dispatch strategy for power–water networks, IEEE Trans. Control Syst. Netw. 9 (1) (2021) 356–366.
[65] Y. Duan, Y. Zhao, J. Hu, An initialization-free distributed algorithm for dynamic economic dispatch problems in microgrid: modeling, optimization and analysis, Sustain. Energy Grids Network 34 (2023) 101004.
[66] D.A. Wood, Spatio-Temporal Attributes of Varicella Zoster Case Number Trends Assist with Optimizing Machine Learning Predictions, Medinformatics, 2023.
[67] M. Shirkhani, J. Tavoosi, S. Danyali, A.K. Sarvenoee, A. Abdali, A. Mohammadzadeh, C. Zhang, A review on microgrid decentralized energy/voltage control structures and methods, Energy Rep. 10 (2023) 368–380.
[68] Y. Yang, X. Wei, W. Yao, J. Lan, Broadband electrical impedance matching of sandwiched piezoelectric ultrasonic transducers for structural health monitoring of the rail in-service, Sensor Actuator Phys. 364 (2023) 114819.
[69] Q. Zhang, J. Xiao, C. Tian, J. Chun-Wei Lin, S. Zhang, A robust deformed convolutional neural network (CNN) for image denoising, CAAI-Trans. Intell. Technol. 8 (2) (2023) 331–342.
[70] H. Alimoradi, M. Shams, Optimization of subcooled flow boiling in a vertical pipe by using artificial neural network and multi objective genetic algorithm, Appl. Therm. Eng. 111 (2017) 1039–1051.
[71] B. Li, J. Huang, S. Bai, Z. Gan, S. Liang, N. Evgeny, S. Yao, Autonomous air combat decision-making of UAV based on parallel self-play reinforcement learning, CAAI-Trans. Intell. Technol. 8 (1) (2023) 64–81.
[72] H. Alimoradi, E. Eskandari, M. Pourbagian, M. Shams, A parametric study of subcooled flow boiling of Al2O3/water nanofluid using numerical simulation and artificial neural networks, Nanoscale Microscale Thermophys. Eng. 26 (2–3) (2022) 129–159.
[73] H. Zhu, T. Yi, S. Shang, M. Shi, Z. Li, W. Shang, A multiple sensitive attributes data publishing method with guaranteed information utility, CAAI-Trans. Intell. Technol. 8 (2) (2023) 288–296.